Beam Performance

Beam Performance and Upgrades of the Storage Ring

Top-up Operation

The top-up operation at the SPring-8 was started in May 2004. In this operation mode, the beam is injected every one minute or every five minutes to maintain the stored current at a maximum of 100 mA. The stored current in the top-up mode is kept constant with a deviation less than 0.1%. Thus the top-up operation yielded considerable profit for users, for example, increment of average radiation intensity, stabilizations of the intensity and the constant heat load on experimental equipments, and so on [1].

In order to make the top-up operation available to user experiments, we had to overcome cruxes in beam injection with an open photon beam shutter. The most serious problem is injected beam loss since an open photon beam shutter permits the bremsstrahlung from lost electrons to be transported into the experimental hall. Furthermore, there is the fear of the demagnetization of insertion devices (IDs) due to the lost electron bombardment during beam injection with a closed gap. Through the study of the injected beam loss process, we found that the injected electrons with large horizontal amplitude are not captured in the storage ring [2]. For the purpose of disposing of troublesome lost particles in the beam tail, a collimation system for the injected electron beam was installed at the beam transport line from the booster synchrotron to the storage ring (SSBT). The collimation system consists of two pairs of collimators (SL1A_ss and SL1B_ss), which were placed on a dispersion-free section in the SSBT. Because of the negligible dispersion, the collimators can only be used for betatron collimation. In order to limit x and x' in the betatron phase space, the horizontal phase difference between SL1A_ss and SL1B_ss were designed to be $\pi/2$. For both collimators, two stainless-steel plates 21.2 mm thick were prepared as left- and right-side blades. An optical transition radiation (OTR) on the surface of the blade was observed using a CCD camera. Figure 1 shows that beam tails on the blades were observed. To determine the relation between injection efficiency and the collimator gaps, the efficiencies with various gaps were measured [3]. Figure 2 shows the effect of the collimator on the efficiency of injection to the storage ring. Even under the condition that all ID gaps are close to the minimum, a high injection efficiency of over 80% is achieved with the use of the collimator when the half-gap width is set to 1 σ (standard deviation) of the injected beam distribution.

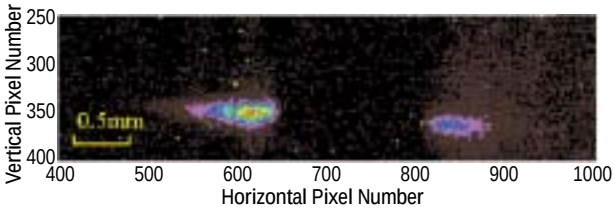

Fig. 1. Relative intensity distribution of OTR at the surface of SL1A_ss. Red and black points indicate the highest and the lowest intensities, respectively. Scale is 8.1 μm/pixel.

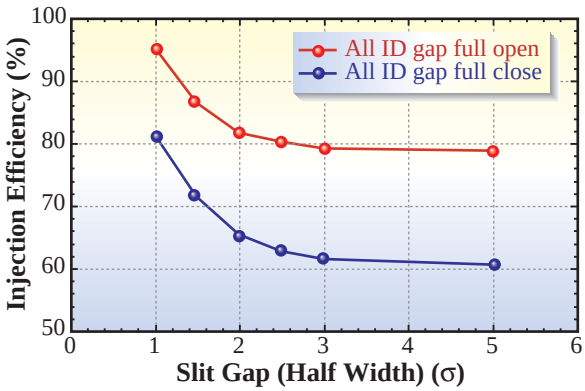

Fig. 2. Dependence of injection efficiency on slit gap of SSBT collimator. The gap width of the collimator is measured from the beam size of the injected beam.

For the top-up operation, it is also important that beam injection dose not excite orbit variation of the stored beam in order not to disturb user experiments. If the injection bump orbit is not completely closed, the stored beam suffers an error kick while passing through the bump orbit. We found that the excitation occurred due to the non-similarity fields of bump magnets and the non-linear field of sextupole magnets within the bump orbit, and that this non-similarity of bump magnet fields originates from the eddy current generated in the metallic end plates of bump magnets. The excitation of the stored beam orbit variation by the non-linearity of the bump

magnet field was hence avoided by replacing the bump magnets with new ones having non-metallic end plates [4]. In order to suppress the stored beam oscillation excited by a sextupole non-linear field, we have developed novel optics for the storage ring [5]. We also measured the vertical oscillation excitation of the stored beam by beam injection to the storage ring. We found that the amplitude of the vertical oscillation is proportional to the waveform of the bump magnet field. Hence we correct the vertical oscillation of the stored beam orbit by tilting two of four the bump magnets. After the main portion of the stored beam orbit oscillation excited by the beam injection was improved by the above countermeasures, the corrector bump magnets were installed to reduce the residual oscillations in both horizontal and vertical directions. The improvements of the stored beam orbit oscillation excited by beam injection in the horizontal direction is shown in Fig. 3. These oscillations excited by the injection bump are measured using turn-by-turn beam position monitors. The horizontal and vertical oscillation amplitudes of the stored beam induced by the injection bump are reduced to one-third and two-thirds of the beams, respectively. At present, the excited oscillation of the stored beam gives negligible disturbance to users.

To deliver beams to user experiments with the top-up operation, a new interlock logic was necessary; the amount of lost electrons during injections to the storage ring in the top-up operation must be controlled. The integration of lost electrons at the time of injection during one week should not exceed the value permitted for the top-up operation. An interlock system was installed to deal with the top-up operation requirements. The amounts of loss are calculated from the difference between injected charges and the increment of the stored current of the storage ring. The injected charges are measured with integrated current transformers (ICT) combined with beam charge monitors (BCM) installed in the most downstream part of the SSBT. The stored current of the storage ring is measured with direct current current transformers (DCCT). Data taken with these devices are sent to a programmable logic controller (PLC), and logics inside the PLC judge the condition and issue an interlock signal when necessary.

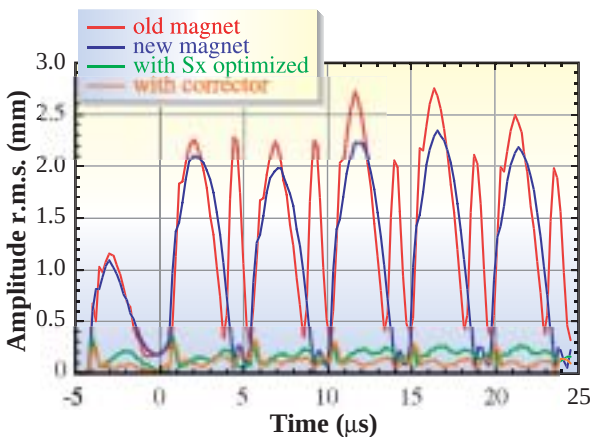

Fig. 3. Improvement of stored beam oscillation excited by injection bump in horizontal direction. The origin of the abscissa in the figure corresponds to the peak of the bump waveform.

In non-top-up operation, a slow drift of the electron beam orbit, the magnitude of which is approximately 10 μm per week, is observed even though the orbit correction is performed with about 250 normal steering magnets (NSTs) before and after beam refilling. Since top-up operation is continuous over a long period, about two or three weeks, suppression of the slow orbit drift is quite important for user experiments. To solve this problem, a greater number of special steering magnets with high setting resolution (HRSTs) are required. To this end, we conceived an idea to make NST function as HRST merely by improving the power supply system of NST. We succeeded in the modification of the power supply system to achieve the current setting resolution of 21 bit by introducing double remote IO units [6]. By the beam test for checking the basic performance, we carried out the improvement of the periodic orbit correction system based on the modification of the NST power supply system to provide another 48 HRSTs for the correction system. By this change, the number of HRSTs in each plane was increased from 24 to 48. Figure 4 shows the orbit stability during the top-up operation over 1 week after the improvement of the periodic orbit correction system. The long-term stability of the orbit is dramatically improved by both this improvement and top-up operation compared with the stability in the case of non-top-up operation.

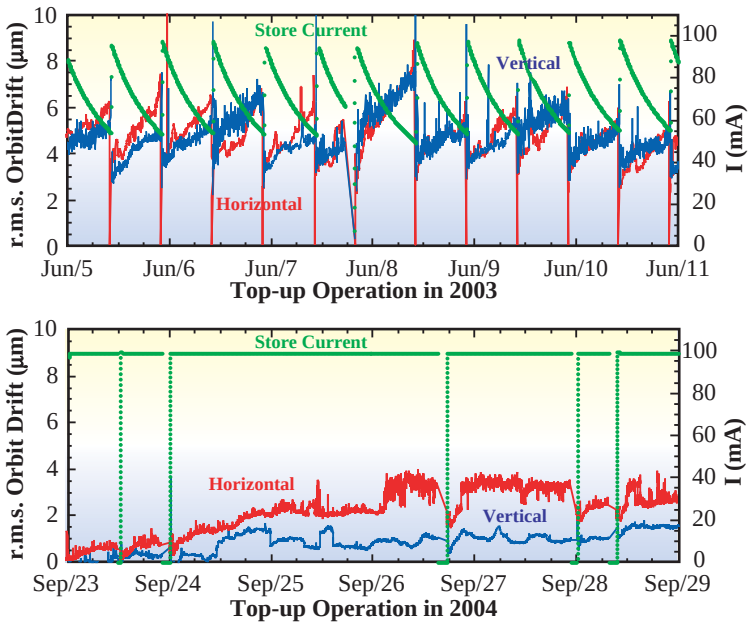

Fig. 4. Long-term stability of electron beam orbit over one week. The upper and lower graphs show the long-term stability during non-top-up and top-up operations, respectively.

Bunch-by-bunch feedback

A bunch-by-bunch feedback [7] system is developed to suppress the horizontal and vertical beam instabilities that arise during low chromaticity operation for the top-up operation of the ring or for future high bunch current operation. The feedback has been in operation in the user mode from the beginning of 2004 without any trouble or any additional tuning during the current year. The measured feedback damping time is less than 1 ms, which is one order faster than that of radiation damping, 8 ms. The noise in the beam position propagates through the feedback to the kicker and excites the beam motion. To reduce this residual motion to less than one-tenth of the beam size, 1 μm, the feedback is made by a low noise system using a newly developed high-resolution beam position monitor of single pass resolution 5 μm and 12-bit ADCs with a new concept analog demultiplexer. Any degradation of the beam quality is observed and reported by users. The reconfigurable hardware logic, field programmable gate array (FPGA), is employed for digital signal processing and its one-order-higher processing power than DSPs or CPUs make our system simple, fast and cost effective. Also, with the newly developed FIR filter algorithm for feedback signal production in combination with this FPGA processing power, the system is versatile and flexible and easy to apply to other storage rings. A new board with ADCs, DAC and a single FPGA that processes both FIR filters, and a multiplexer is being developing to reduce the number of tuning parameters for easy tuning, control and maintenance (Fig. 5).

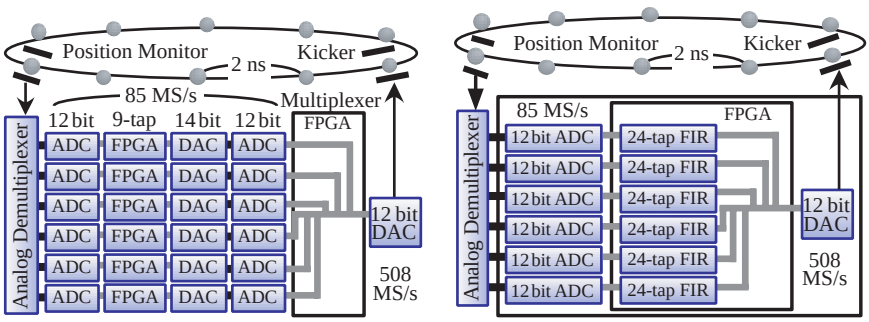

Fig. 5. Current system (left) and new system under development (right).

Accelerator Diagnostics Beamlines

Diagnostics of the electron beam for storage ring tuning towards the realization of ideal top-up operation have been performed at the diagnosis beamline I (BL38B2) using visible and X-ray synchrotron radiation (SR). Information on the bunch impurity and the beam current of each bunch is important for the top-up operation in several-bunch modes. The evolution of bunch impurity during the top-up operation has been measured using the gated photon-counting system with fast light shutters in the visible light region. An example of the variation of the bunch impurity, which is the ratio of the number of electrons in the bucket adjacent to the target bucket on the trailing time side to that in the target bucket, during one week of top-up operation is shown in Fig. 6. The increase of the impurity to the level of 2×10^{-9} was observed during one week, which is a sufficiently small level for user experiments.

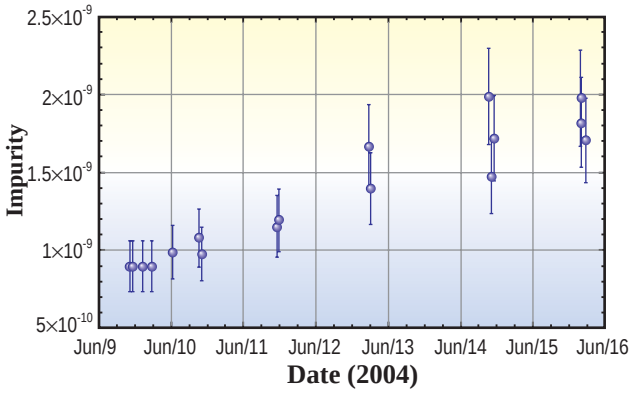

Fig. 6. Observed variation of bunch impurity during top-up operation.

The transient behaviors of the effective beam profile after beam injections have been measured by the X-ray beam imager (XBI) based on a Fresnel zone plate and an X-ray zooming tube. The time variation of effective horizontal and vertical beam sizes normalized to the values of the damped beam, which were measured in the top-up operation, are shown in Fig. 7.

Construction of the accelerator diagnosis beamline II (BL05SS) is in progress. The beamline has a straight section for IDs. An ID with flexibility for exchanging magnet arrays has been designed to provide a variety of SR for various kinds of

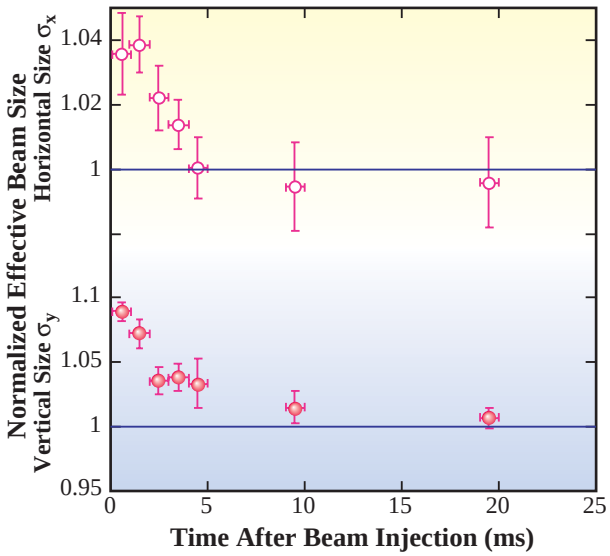

Fig. 7. Time dependence after beam injections of horizontal and vertical effective beam sizes in top-up operation obs erved by XBI. The integration time is 1 ms. The beam sizes are normalized to values of the damped beam which were measured between injections.

experiments. It has a C-shaped magnet support structure of an out-vacuum type. The magnet support structure can be moved off the electron beam axis to the maintenance position by sliding it on guide rails (Fig. 8), so that magnet arrays can be exchanged easily. The slide system will be installed in a pit and embedded below floor level. A magnet array of multi-pole wiggler (MPW) type has been designed to produce high-power SR for the purpose of studying radiation damage to accelerator components and developing of high-heat-load components such as photon absorbers. The period length and the period number are 76 mm and 51, respectively. At the minimum magnet gap of 20 mm, the deflection parameter K is 5.8, and the total power and peak power density are 10 kW and 200 kW/mrad^2, respectively, for the beam current of 100 mA. The ID and the ID vacuum chamber will be installed in summer of 2005.

A compact photon absorber for the front-end has been developed, which withstands high heat load of the SR from the MPW. To make the absorber compact, two absorber blocks made of Glid-Cop with different tilt angles of the surface have been arranged in tandem in the vacuum chamber. The front absorber intercepts the upper and lower parts of SR, and the rear one absorbs the central part of SR. The photon absorber will be installed in the front-end also in the summer of 2005.

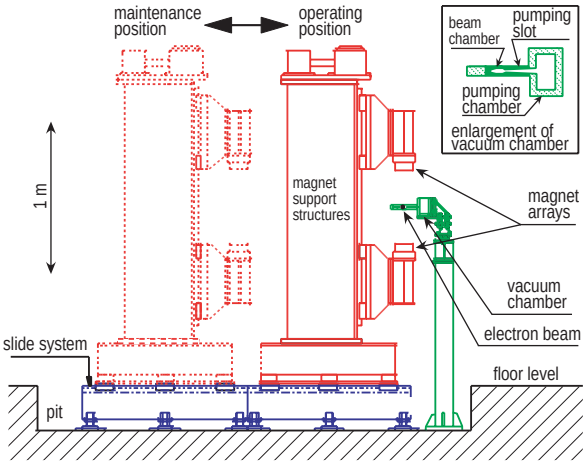

Fig. 8. Schematic of ID of accelerator diagnosis beamline II.

Other Topics

Damage of the injection chamber by aborted electron beam

The stored electrons in the storage ring should be aborted using the safety interlock. RF power supply would be turned off because the stored electrons should be aborted as soon as possible. The radius of electron orbits decreases and the electrons finally vanish on the chamber wall. The storage ring was operated with low-emittance optics between autumn 2002 and autumn 2003. In this case, most aborted electrons hit the thin stainless-steel wall (0.7 mm thickness of SUS316L) of the injection vacuum chamber. During the passage through the chamber material, electron energy is converted to heat by growth of the electromagnetic shower: the cascade reactions of bremsstrahlung, electron positron pair creation, multiple scattering and the ionization of electrons and positrons. The small electron beam size corresponds to the highly localized high-heat-load on the chamber. In October 2003, the thin wall of the injection chamber was broken due to such large heat load and vacuum leakage occurred as a result of the deformation and the cracking of the chamber wall due to the residual stress. Figure 9 shows the damaged thin wall of the vacuum chamber and etched cross sections of the damaged part. On the surface of the thin wall, some straight lines are seen, cause by the oxidization of stainless-steel due to the high-heat-load of electron beam passage. On the cross section, there are several features that are evidence of heat load: holes due to the meltdown, and resolidified solids after meltdown or semi-meltdown. These observations indicate that the aborted electrons hit the thin wall several times.

The damaged vacuum chamber was replaced by a spare one. Since October 2003, the normal-emittance optics has been employed for user time operation. A new injection chamber with an electron beam damper made of aluminum has been designed and is under construction. It will be installed in the summer of 2005, and the ring optics will be changed to a low-emittance optics.

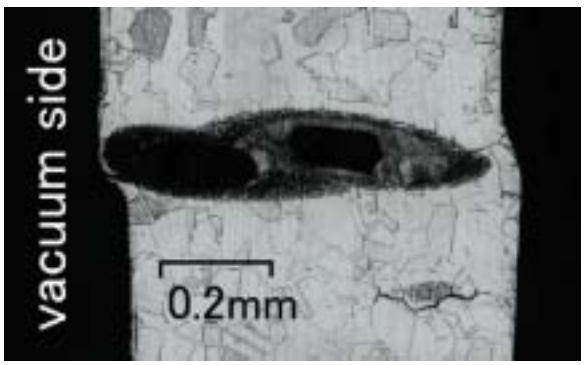

Fig. 9. Details of cross-section of stainless-steel chamber wall at the broken part.

HLS System [8]

In order to measure very slow ground movement over a wide area, a 50-meter-long hydrostatic leveling system (HLS) has been set up in the storage ring tunnel above a vehicle underpass. The system has 6 sensors at intervals of 5 or 10 m. The long-term movement from January to November of 2004 is shown in Fig. 10. It is clear that the level of the tunnel floor changes seasonally. The floor begins to rise from the lowest position in March and reaches the highest position in September. The level difference is 0.25 mm. The rate of change is 2 μm/day in June and July. The underpass is a π-shape structure 8-meters wide and 6-meters high viewed from the passage. The shape of this structure is considered to depend on the temperature gradient between the passage side and the inner tunnel or underground. The deformation occurs because of the expansion of sidewalls and bending of the floor.

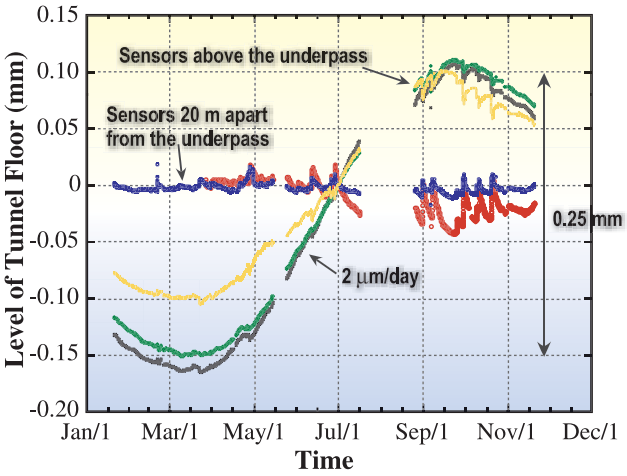

Fig. 10. Long-term movement of the tunnel floor above the vehicle underpass. The level changes by 0.25 mm from late March to September 2004. The rate of change is 2 μm/day.

Developments and Upgrades of Linac

Improvements towards top-up operation [9]

The SPring-8 linac has been improved since 1998 in order to provide beams with the stable energy and current; the energy stability has since been enhanced to 0.01% rms [10]. Temperature fluctuations in the klystron gallery, however, have not been negligible since 2002 when electric power saving of the linac began. We reduced the RF repetition rate from 60 Hz to 10 Hz for electric power saving in 2002 and accordingly observed remarkable room temperature drift in winter when the outdoor air temperature was low. These temperature variations caused the RF phase variations, as we experienced before 1998. The beam energies during acceleration from a buncher system to the end accordingly varied slightly, resulting in a distortion of the beam trajectory. We therefore investigated this room temperature issue to stabilize the trajectory fluctuations. The final beam energy, however, was stabilized by an energy compression system (ECS). The long-term energy stability was measured using BPM and OTR monitors. Figure 11 presents the beam energy variations before and after the ECS during a period of two days. The plotted energies before show the accidental reduction; the compensated energies, however, maintained the stability of 0.14% (p-p) throughout the measurement. Thus the ECS is effective in maintaining both shot-by-shot and long period beam energy stability.

The Linac is equipped with a bending magnet which switches a beam from the transport line for the New SUBARU storage ring to one for the booster synchrotron. In order to perform simultaneous top-up operation of the two rings, the previous block-type bending magnet was replaced with a fast-response bending magnet which could be momentary excited at short intervals. The new bending magnet must repeatedly turned on and off at short intervals to inject the beams frequently into both the synchrotrons. In order to achieve fast response and a small residual field, a 50A400 silicon steel plate 0.5 mm thick was chosen for the lamination-type yoke of the new magnet. The measured residual field was about 10 gauss, one-third of the previous field. A fast-response power supply was also fabricated for the new bending magnet. This power supply can excite the new magnet at 0.9 T with the rise/fall time of 200 ms.

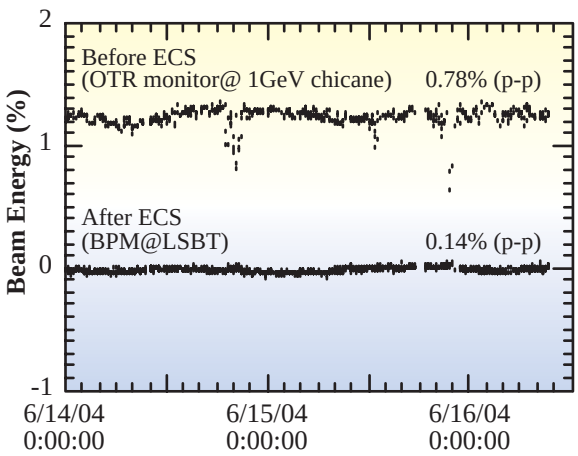

Fig. 11. Variations of the beam energy before and after ECS.